Catalysis Today 172 (2011) 218–225

Contents lists available at ScienceDirect

Catalysis Today

journal homepage: www.elsevier.com/locate/cattod

The influence of different methanol synthesis catalysts on direct synthesis of DME from syngas

J.H. Flores [a], D.P.B. Peixoto [a], L.G. Appel [b], R.R. de Avillez [c], M.I. Pais da Silva [a,*]

[a] Departamento de Química, Pontifícia Universidade Católica de Rio de Janeiro, Rua Marquês de São Vicente 225, Gávea, Rio de Janeiro, CEP 22453-900, Brazil
[b] Laboratório de Catálise, Instituto Nacional de Tecnologia/MCT, Av. Venezuela 82/507, Rio de Janeiro 22081-312, Brazil
[c] Departamento de Engenharia de Materiais, Pontifícia Universidade Católica, Rua Marquês de São Vicente 255, Gávea, Rio de Janeiro 22453-900, Brazil

ARTICLE INFO

Article history:
Received 1 December 2010
Received in revised form 18 February 2011
Accepted 28 February 2011
Available online 13 April 2011

Keywords:
DME
Methanol
Zr
Cu–Zn–Al catalyst

ABSTRACT

Methanol synthesis catalysts based on Cu–Zn–Al prepared under different precipitation conditions with the use of Zr or not as a promoter were studied in the direct synthesis of dimethyl ether (DME) using H-ferrierite as a dehydration component. Samples prepared under high supersaturation conditions showed textural and structural changes without any relation to the CO conversion. Samples containing zirconium favored an increase of Cu surface area, but other factors were involved in the improvement of the catalyst activity. The presence of aluminum in the methanol synthesis catalyst produced structural changes that could be related to the catalytic activity.

1. Introduction

Dimethyl ether (DME) is an important chemical and has received significant attention as a clean fuel source. DME can be synthesized from natural gas, coal and agricultural residues. The application of DME as an alternative to diesel fuel has been proposed because of its lower NO_x emission and its near-zero smoke evolution compared to traditional diesel fuels [1–4].

Three reactions are involved in DME production from synthesis gas: (i) methanol formation, (ii) the dehydration of methanol to DME and water and (iii) the reaction of water with CO to form CO_2 and H_2 through the water-gas shift (WGS) reaction. The direct synthesis of DME has been presented using a bifunctional catalyst that contains two active sites; one site is utilized for the methanol synthesis and the other for DME formation via the dehydration of methanol [5–9]. Cu-based catalysts have been widely used in methanol synthesis. The Cu–ZnO–Al_2O_3 system in particular has been studied by many researchers and has shown the best results [10,11].

Acidic components, such as γ-Al_2O_3, H-ZSM-5 or HY zeolites, are widely used as dehydration components and exhibit similar activities [12]. In addition, the rate of DME synthesis has been defined by the acidic properties of the dehydration component [13]. The pure acid component was not expected to show activity toward the direct transformation of the synthesis gas to methanol or DME [14]. Recently, the superiority of ferrierite over other zeolites has been demonstrated, primarily due to its acidity, suitable topology and the facile reducibility of its metal components [15,16].

To enhance methanol production and the DME yield, highly active methanol synthesis catalysts have been prepared. The Cu–Zn–Al oxide-based catalysts are usually prepared by the conventional coprecipitation method with the aim of forming a hydrotalcite-like precursor [17]. The evolution of the copper particles depends on the preparation conditions, such as the pH, Cu/Zn mole ratio, the addition of reagents and heat treatments during and after the precipitation. The addition of small amounts of tri- and tetra-valent ions can produce cationic defects in the structure, which can enrich and stabilize copper on the surface of the catalyst [18].

Textural, morphological and structural theories have been put forth to explain the active site responsible for the activity in methanol synthesis. In general, the Cu surface area is considered to be primarily responsible for methanol synthesis activity, with highly dispersed copper providing even higher activity. The role of ZnO would be to increase this dispersion [19]. According to some authors, the Cu surface area alone cannot be considered responsible for the methanol production rates. They proposed that Cu strain produced by structural defects, incomplete reductions or Cu epitaxial orientation due to the ZnO may modify the Cu surface area and influence the catalytic activity [20]. Others authors have proposed that a series of effects, including epitaxial strain, shape dynamics and Cu–Zn alloy formation that was created when the Cu/ZnO was

* Corresponding author. Fax: +55 21 35271323.
E-mail address: isapais@puc-rio.br (M.I.P. Silva).

0920-5861/$ – see front matter © 2011 Elsevier B.V. All rights reserved.
doi:10.1016/j.cattod.2011.02.063

reduced, is responsible for the special metal-supported interaction of Cu/ZnO [21,22]. The synergy between the Cu and the ZnO is believed to be related to the kind of interaction between the metal and the support. Conversely, according to Fujita et al. [19], Cu–Zn alloy formation is related to the ZnO content and its presence could be directly related to specific activity in methanol synthesis.

Several studies on the influence of metallic promoters on methanol catalysts have shown that Zr is the more efficient promoter but its role is still not clear. Zirconium has been found to improve Cu dispersion and can lower the Al content on the catalyst surface [23], while Cu and Zr have a synergistic interaction that facilitates the reduction of Cu^{+2} [24]. Furthermore, the presence of Zr or Al can provide a high stability and resistance to redox cycles [25]. The higher activity of the Cu–Zr-based catalysts has also been attributed to the stability of Cu_2O on the surface of the reduced catalyst during the reaction [26]. Conversely, it has been reported that a low degree of microstrain in the Cu particles is produced when the catalyst is supported on ZrO_2 [27].

Herein, methanol synthesis catalysts based on Cu–Zn–Al were prepared by the coprecipitation method while varying the temperature and the mixture of reactants. The addition of Zr in place of Al or as a fourth element in the mixture was also investigated. These catalysts were physically mixed with H-ferrierite zeolite for the direct synthesis of DME from syngas. The activity of the various methanol synthesis catalysts via a single-step DME synthesis was investigated.

2. Experimental

2.1. Catalyst preparation

Several methanol synthesis catalysts (MSCs) prepared by different methods were physically mixed with ferrierite zeolite. This zeolite (Si/Al = 10) provided by Toyo Soda Manufacturing, serial number 720 KOA, was used in its acid form. The ions, Na^+ and K^+, were exchanged using an ammonium acetate solution at 90 °C. The zeolite was calcined in air at 500 °C (10 °C min^{-1}) to produce the zeolite in the acidic form (H-Fer). The most important properties of this material were the surface area (314 m^2 g^{-1}), micropore volume (0.18 cm^3 g^{-1}), medium pore diameter (17.4 Å) and Bronsted/Lewis acid sites (ratio determined by pyridine adsorption of 7.7) [28].

The following preparation methods were used to prepare the methanol synthesis catalysts: the coprecipitation was performed using a low supersaturation method (LS-80) based on the slow (30 min) and simultaneous mixture of two solutions, one containing nitrates of Cu, Zn and Al (1.0 mol dm^{-3} and Cu/Zn/Al = 55/30/15 atomic ratio) and another containing Na_2CO_3 (1.5 mol dm^{-3}), at 80 °C under vigorous stirring at ~pH 8. The precipitate formed was aged in the mother solution for 1 h at 80 °C, which was an appropriate amount of time to form the crystalline phase precursor [29]. It was then washed with warm water (1 L) to eliminate the Na and nitrate residues, dried for 12 h at 90 °C and calcined for 4 h at 400 °C in a N_2 atmosphere. The coprecipitation consisted of a fast mixture (few seconds) of the two above solutions using a high supersaturation method. Two catalysts were prepared using this method; one was prepared using the solutions at 25 °C and other with the solutions warmed to 80 °C; the samples were named HS-25 and HS-80, respectively. The precipitates were aged at the same temperature as the mixture and later washed, dried and calcined as before. The fourth method utilized, called high pH, consisted of the slow addition of a solution of Cu, Zn and Al nitrates to an aqueous solution of Na_2CO_3 warmed at 80 °C under intense stirring. The solid material was then aged, washed, dried and calcined at same above conditions. Methanol synthesis catalysts were also prepared based on Cu–Zn–Zr and Cu–Zn–Al–Zr by the coprecipitation via the low supersaturation method and were named CZZr and CZAZr with atomic ratios of 55/30/15 and 50/27/13/10, respectively. A commercial catalyst used for methanol synthesis (Katalco) was utilized as a comparison and mixed with the H-ferrierite zeolite. The MSC/zeolite weight ratio used for all catalysts was 4:1.

2.2. Characterization

The BET surface area, pore diameter and pore volume were measured by the N_2-physisorption at −196 °C using a Micrometrics ASAP 2000. Prior to the adsorption-desorption measurements, all samples were degassed at 250 °C.

A Rigaku diffractometer with CuKα radiation and a tension of 40 kV was used for the X-ray measurements of the precursors and the calcined catalysts. The angle 2θ covered was between 5° and 60°. The quantitative phase content and crystallite sizes were determined by a multiphase Rietveld refinement using Topas software and a fundamental parameter approach for modeling the peak shape. Samples reduced were also analyzed by X-ray diffration (XRD). The samples were reduced *ex situ* at 250 °C during 1 h using pure H_2 and after passivated with O_2/He (3%), at 30 mL min^{-1} and 25 °C during 1 h. After the passivation the samples were manipulated sob inert atmosphere (N_2) and analyzed immediately.

The temperature programmed desorption of H_2 technique (H_2-TPD) was used to determine the Cu surface area and was adapted from Mühler [30]. A TPR/TPD conventional apparatus equipped with a Baltzer Mass Quadrupole was used for analysis of the samples, which were inside a quartz reactor with a thermocouple and a furnace. The samples were first dried with pure He up to 150 °C and kept at this temperature for 1 h before being reduced with pure H_2 (60 mL dm^{-3}) at 250 °C (heating rate of 10 °C min^{-1}) for 1 h. After the sample was cooled to room temperature, it was cooled to 0 °C using an ice bath and maintained at this temperature for 1 h. The samples were then cooled to −196 °C for 1 h using a liquid nitrogen bath. Subsequently, the H_2 flow was switched to a 50 mL dm^{-3} He flow for 30 min at this temperature. After the sample was removed from the bath, it was heated at 50 °C min^{-1} from room temperature to 350 °C. The hydrogen desorption was monitored through the $m/z = 2$. H_2-TPD profiles presented two overlapping peaks of desorption; a very large peak was present at approximately 25 °C and the very small peak at lower temperature had no effect on final result obtained using the total area.

The morphology and structure of the calcined and reduced catalysts were investigated by transmission electron microscopy (TEM) using a JEOL 2010 operating at 200 kV. Samples were dispersed into isopropyl alcohol and then deposited over a grid to be observed by the microscopy.

The temperature programmed reduction experiments (H_2-TPR) were conducted using a gas mixture of 1.53 vol% H_2 in Ar. The feed flow rate was 20 mL min^{-1} and the heating rate from room temperature to 600 °C was 5 °C min^{-1}. The hydrogen concentration was determined using a thermal conductivity detector.

2.3. Activity evaluation

The reactions in the gaseous phase were performed in a catalytic test unit equipped with tubular fixed-bed reactor (50 mL volume). The reaction products were analyzed on-line with a gas chromatograph equipped with a thermal conductivity detector (TCD) and a PORAPAK-QS packed column (30 m).

The catalysts were pre-treated with a He/H_2 (5% H_2) mixture at 30 mL min^{-1} for 1 h. The temperature was raised from room temperature to 250 °C at 5 °C min^{-1} under atmospheric pressure. After the reduction step, the reactor temperature was maintained at 250 °C and a total flow of 24 mL min^{-1} of a mixture of 2:1 H_2 and CO was introduced into the unit, which was controlled by mass

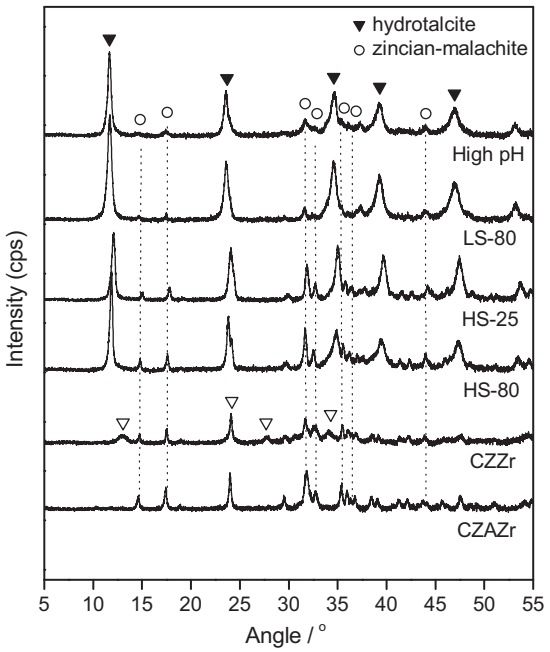

Fig. 1. XRD patterns of precursors of the catalysts.

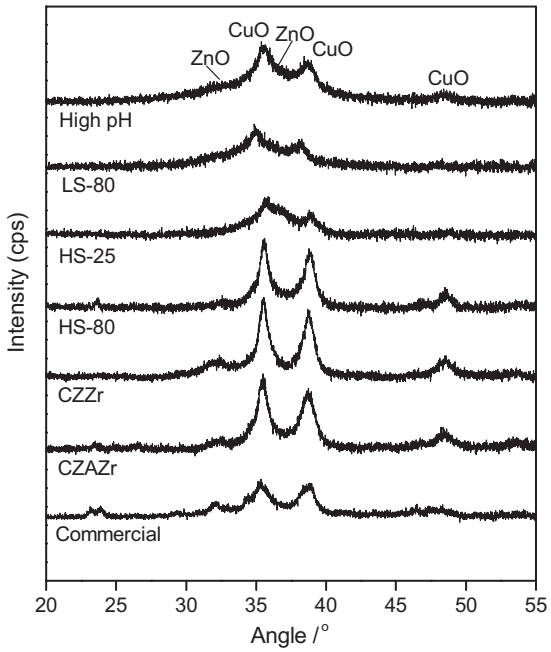

Fig. 2. XRD patterns of the calcined catalysts.

flow controllers. The pressure in the reactor was then increased to 5 MPa. To obtain a fair comparison of each of the catalysts used, the total mass of each was normalized to 200 mg. The reactor stream was analyzed after 170 min of reaction time, which was enough to reach a steady state. The selectivity was calculated for both high and low conversions.

3. Results

3.1. Composition, textural and structural properties

The elemental composition of the MSCs is shown in Table 1. Some differences can be observed in the percentage of metals in the samples due to the different precipitation conditions; however, the atomic ratio among the metals was very similar to the planned ratio. From the obtained results, it was possible to affirm that under the precipitation conditions used, the zirconium was precipitated. The commercial catalyst showed different copper amounts compared to the prepared ternary catalysts.

The results of the BET surface area, pore volume, average pore diameter and copper surface area determined by H_2-TPD are also shown in Table 1. These results corresponded to only the MSC and not to the hybrid catalyst. Clearly, the preparation method had an influence on the textural properties. It is possible that the high supersaturation conditions produced higher surface areas because smaller particles sizes were formed. The addition of Zr in place of the Al or as the fourth metal element in the sample also favored an increased BET surface area. The highest pore volume observed in the CZAZr sample can be attributed to the different intragrain structure of this material due to the small particle sizes. Conversely, a higher average pore diameter was found in the LS-80 ternary catalyst.

The XRD pattern of the precursor samples revealed diffraction lines with hydrotalcite-like structures in all of the ternary samples that were based on Cu–Zn–Al. There was no influence of the preparation method on the phase formed; however, some reflections belonging to the zincian–malachite phase were observed in the samples, as shown in Fig. 1. The presence of a zincian–malachite phase would be due to Cu^{+2} ions showing the Jahn–Teller effect, which favors the formation of distorted octahedral structures and gives rise to the precipitation of malachite phases [31].

The hydrotalcite phase was not observed in the samples that were based on Zr. Lines corresponding to the zincian–malachite phase were observed, and some reflections of the aurichalcite phase were found in the CZZr sample precursor. These results indicated that the tetra-valent ion produced structural changes that did not favor the hydrotalcite formation.

After calcination, the hydrotalcite structure collapsed to form oxidized phases, as shown in Fig. 2. In this figure, peaks belonging to CuO and ZnO phases can be observed. These peaks were more intense in the HS-80, CZZr and CZAZr samples, but broader, less intense and overlapped in the other samples. According to Guo et al. [32], this finding is a characteristic of nanosized material. Kurr et al. [33] also observed an increase of the background in the 30–37° range with the ternary catalyst, which indicated the presence of either highly nano-crystalline or X-ray amorphous ZnO. Peaks belonging to the Al or Zr oxidized phases were not observed, which can be explained by the presence of these oxides in an amorphous state or highly dispersed in the catalyst. Zirconium as a third metallic element or as a tetra-valent promoter in the ternary catalyst did not favor the formation of amorphous-like or less ordered structures, as determined by Zhao et al. [34].

Table 1 also shows the crystallite sizes obtained from the Rietveld refinement method of the calcined and reduced samples. As shown in the table, Zr in place of Al promoted the growth of CuO crystallites; this finding is in contrast to the results obtained by Matsumura et al. [35].

When these catalysts were reduced, an increase in the Cu crystallite size was observed in the samples, with the exception of the HS-80 and CZZr. This increase was due to a sintering process during the reduction. This process was eliminated in the CZZr sample probably because the ZrO_2 stabilized the copper and prevented the crystallite growth [25]. The crystallite size of the pure CuO without promoters was 32.7 nm before reduction and 66.2 nm after reduction. The results indicated that the promoter favored the growth of Cu during the reduction process. The ZnO crystallite size was determined to be 4 and 5 nm in the calcined and reduced samples, respectively.

Table 1
Chemical composition and textural and structural properties.

Sample	Metal (weight %)				Area ($m^2\ g^{-1}$)		Crystallite size (nm)		Average pore diameter $(nm)_{BJH}$	Pore volume (cm^3/g)	Dispersion (%)
	Cu	Zn	Al	Zr	BET	Cu	CuO	Cu			
High pH	31.4	16.7	8.4	–	110	8.3	5.9	6.8	11.3	0.35	14.6
LS-80	39.5	20	10.5	–	50	9.9	7.5	9.9	22.6	0.26	13.9
HS-25	32.3	17.4	8.5	–	92	3.8	4	10.1	9.6	0.23	6.5
HS-80	34.1	17.5	8.9	–	133	8.7	13	12	8.7	0.31	14.2
CZZr	37.5	17.5	–	9.9	100	11.1	16.3	13.2	10.8	0.28	16.3
CZAZr	47.1	20.4	4.9	5.3	95.3	12.9	10.4	15.9	18.9	0.47	19.3
Commercial	40.4	19.7	5.2	–	119	15.3	7.2	9.1	9.2	0.29	21.0

Based on the crystalline phase results (Table 2) and the XRD patterns, the ZrO_2 species was primarily found in the quasi-amorphous form in the calcined samples, which was consistent with results obtained by Sloczynskia and co-workers [36].

3.2. Temperature programmed reduction results

The H_2-TPR profiles of the calcined catalysts and the quantitative evaluation of their peaks are reported in Fig. 3. The amount of consumed hydrogen corresponded to an oxidation state of Cu(II) in practically all materials. Samples prepared under different precipitation conditions were reduced at higher temperatures and exhibited one peak with or without shoulders or two reduction peaks. The high pH sample showed a broad reduction peak, while samples based on Zr reduced at lower temperatures and the commercial catalyst exhibited one reduction peak and a small reduction shoulder. Kurr et al. [33] determined that one reduction stage corresponded to a homogeneous size distribution of CuO particles. The presence of more than one reduction signal in the TPR profiles of $Cu/ZnO/Al_2O_3$ catalysts was already observed and explained by different mechanisms. Some authors have interpreted the different reduction peaks as different Cu(II) species, such as CuO, $CuAl_2O_4$, and Cu^{2+} ions incorporated on the octahedral sites of the Al_2O_3 phase [37–39]. It has also been suggested that two peak profiles represent a two-step reduction: $Cu(II) \rightarrow Cu(I) \rightarrow Cu(0)$, [40]. The two reduction steps of Cu(II) did not seem to be distinguishable by the TPR technique when the Cu(II) species were highly concentrated. This result could be due to (i) a broadening of the peaks in the presence of high amounts of Cu(II) or (ii) the large heat release that increased the temperature of the sample, which sped up the second reduction step [31].

Low reduction temperature indicated small CuO particles and a high dispersion. These results correlated with the Cu^0 surface area measurements because they corresponded to the highest areas found for these catalysts (Table 1). Catalysts based on Cu–Zn–Al required high temperatures for the complete reduction, probably because of a strong interaction between copper and other components.

Table 2
Crystalline phase composition.

Sample	Phase composition determined by Rietveld refinement (%)					
	Calcined			Reduced		
	CuO	ZnO	ZrO2	Cu	ZnO	ZrO2
High pH	62.3	37.8		69.7	30.3	
LS-80	41.5	58.5		83.5	16.5	
HS-25	68.3	31.7		63.0	36.9	
HS-80[a]	65.9	30.3		74.4	25.6	
CZZr	60.2	39.8		59.7	33.3	7.0
CZAZr[a]	70.9	26.4	0.4	68.6	30.1	1.4
Commercial[a,b]	57.7	12.8		52.3	47.7	

[a] Hydroxycarbonated phase 1, HS-80 = 3.7%, CZAZr = 2.3% and Commercial = 7.0%.
[b] Hydroxycarbonated phase 2, commercial = 22.5%.

As described by Agrell et al. [25], large crystallites tend to be reduced more slowly than smaller ones due to their relatively lower surface area exposed to H_2. Therefore, the sintering of copper may be expected for catalysts, such as CZZr and CZAZr, due to the presence of small, reactive particles. However, it appeared that the ZrO_2 effectively stabilized the copper and prevented crystallite growth only in the case of the CZZr sample. Conversely, it seemed that the Al content influenced the reducibility of CuO because of the lower crystallinity of CuO in samples with higher Al content from the XRD results (Fig. 1); these results were in agreement with Velu and co-workers [37]. It was also possible that surface spinel species, i.e., $CuAl_2O_4$, could be easily formed in samples with higher Al content. This species would be reduced at relatively higher temperatures compared with CuO. These results revealed that a decrease in the Al content and its substitution by Zr improved the copper reducibility.

There is evidence that ZnO is reduced above 500 °C [41], although the partial reduction of surface ZnO, which may lead to the formation of α-brass (dilute alloy of Zinc in Cu), cannot be completely discarded. Thermodynamic calculations have shown that

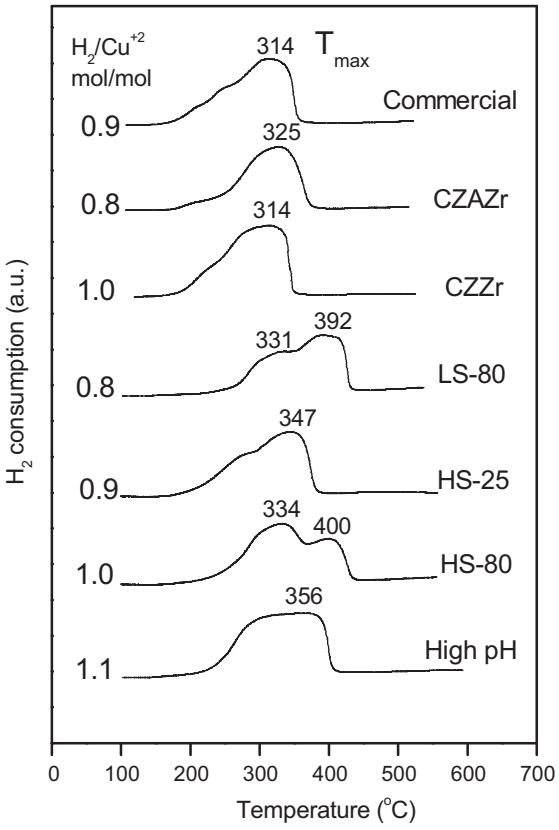

Fig. 3. TPR profiles of the calcined catalysts.

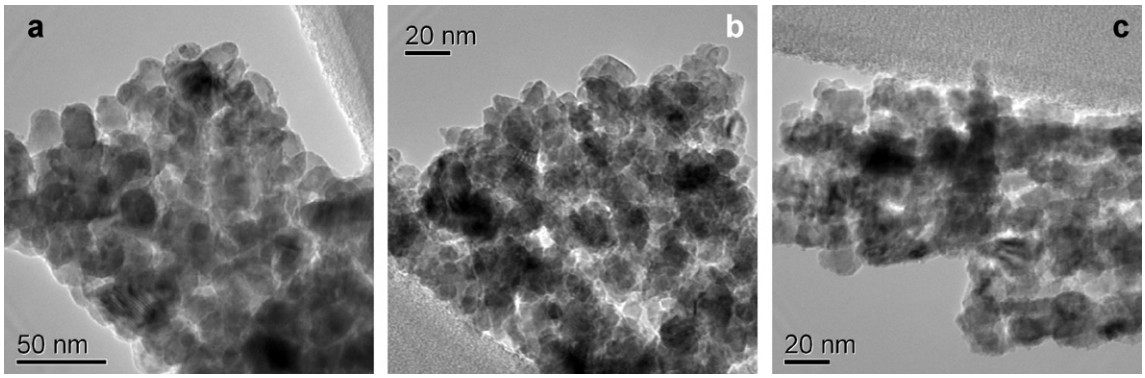

Fig. 4. TEM pictures of the calcined catalyst: (a) HS-80, (b) CZZr and (c) CZAZr.

the equilibrium zinc content in a surface α-brass is approximately 5% during the catalyst reduction at 300 °C [42].

3.3. TEM

The TEM micrographs of three calcined catalysts are shown in Fig. 4. The TEM micrographs revealed agglomerated granular particles with morphological differences among the samples and different particle sizes. The largest particles were found in the HS-80 sample, which showed a regular morphology. The addition of Zr promoted a decrease in particle size, as can be seen in Fig. 4b and c. Additionally, the morphology of the calcined samples that contained Zr was less regular. Some particles presented disk-like shapes, while others showed irregular shapes, primarily in the CZAZr sample.

Based on the TEM images, the Zr promoted small particle size formation and the morphological changes observed could be a product of structural modifications of the CuO–ZnO matrix.

According to Liu and co-workers [43], a smaller particle size resulted in the catalyst possessing more edges, corners, defects and oxygen vacancies. For a structure-sensitive reaction, these would be beneficial to the reaction performance.

3.4. Catalytic activity

The experimental results of the CO conversion are shown in Fig. 5. Samples prepared at high supersaturation conditions presented higher conversions; the highest conversion was observed in the HS-80-HFer sample. The lowest activity was found in the LS-80-HFer catalyst. Zirconium addition under low supersaturation conditions considerably enhanced the activity. This effect was more pronounced in the CZAZr-HFer sample in which the Zr inclusion into the ternary catalyst, based on Cu–Zn–Al, favored the CO conversion. This last result was comparable to the hybrid catalyst based on the commercial methanol synthesis catalyst.

Based on the selectivity results, larger amounts of DME were produced in addition to CO_2. The low content of methanol observed for the hybrid catalysts (below 3%), except the commercial based methanol synthesis catalyst, demonstrated the high capacity of the H-ferrierite zeolite as a dehydration component in the hybrid catalysts. No hydrocarbon by-products were observed in any of the reactions. Some variations can be observed in selectivity at low conversion levels (Fig. 6). The LS-80-H-Fer and Com-HFer catalysts exhibited a lower selectivity toward DME and higher selectivity toward CO_2. There were no appreciable differences in DME selectivity among the different hybrid catalysts for high conversion levels, indicating that the product equilibrium composition had possibly been reached with the reaction conditions that were utilized.

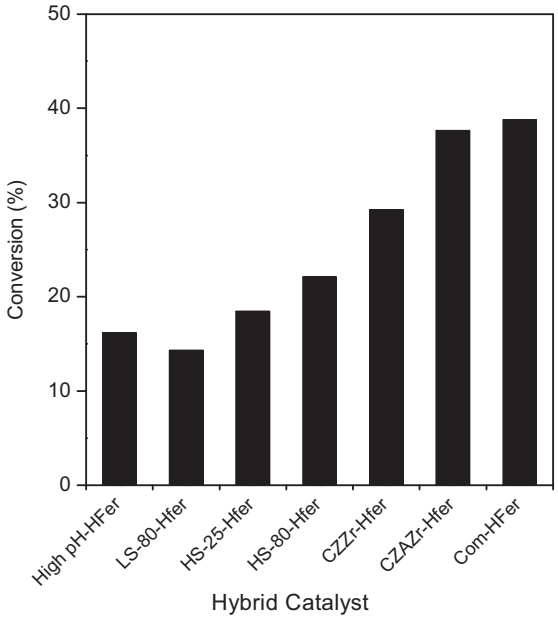

Fig. 5. Performance of the hybrid catalysts.

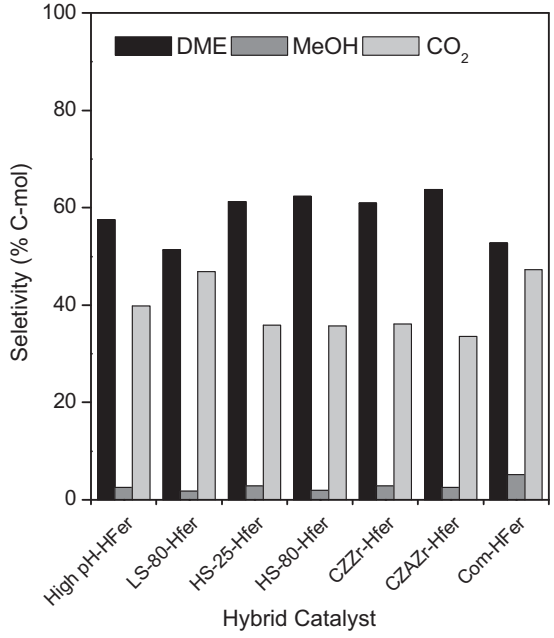

Fig. 6. Selectivity of the hybrid catalysts.

4. Discussion

The greatest variation found in the activity results was in the CO conversion, which was directly related to methanol formation and, consequently, to the methanol synthesis catalyst. In general, the activity of a hybrid catalyst for the DME synthesis from syngas depended on the dispersion of the metallic copper and the number of acidic sites. Therefore, it was possible to affirm that the acidic sites available on the hybrid catalysts were enough to transform the methanol produced in the first stage to DME.

The changes in the precipitation conditions of the methanol synthesis catalysts affected the textural properties, as shown in Table 1. Despite the changes in the BET surface, pore volume and average pore diameter, no direct relation with the copper surface area was found, which was an important variable involved in the catalytic activity. For instance, the lowest BET surface was observed in the LS-80 sample; however, this sample presented the highest copper surface area.

The precipitation method based on varying the pH provided fine grained crystals with rough surfaces and relatively high surface areas, whereas the constant-pH method provided larger well-formed hexagonal crystals. Precipitation at constant pH involved low supersaturation, leading to a relatively small number of nuclei; thus, the larger crystallites were generally produced. This observation was consistent compared to the TEM results found for the LS-80 sample. The process of reactant addition took a considerable amount of time at both varied pH and constant pH; therefore, the initially formed nuclei had more time to undergo the aging process compared to those formed at the end of the addition process. In methods occurring at high supersaturation, a higher number of nuclei were formed and the aging took place without perturbation.

From these results, it can be concluded that with the different precipitation conditions, the Cu surface area was not the principal contributing parameter for the higher conversions. In this case, a structure-activity phenomenon was likely responsible for the catalytic behavior.

The samples based on Zr showed an increase in the area of copper and higher conversions, which was consistent with the findings by Agrell et al. [25] and Breen et al. [44]. The ZrO_2 could promote the synergy between Cu and Zn and possessed oxygen ion vacancies, which produced a geometric effect that could influence the dispersion and alter the morphology of copper particles [45]. It can also improve the dispersion of Cu crystallites and lead to more active sites in the catalysts after reduction [23].

Based on the relation between the copper surface area and CO conversion shown in Fig. 7, it was possible to conclude that a correlation between these two variables existed; however, the correlation was found to be non-linear in some samples. For instance, the highest copper surface area observed in the catalysts based on Cu–Zn–Al showed the lowest conversion of CO. Conversely, samples based on Zr showed a correlation between CO conversion and the Cu metal surface determined by the H_2-TPD, leading to higher DME yields. These results demonstrated that it was necessary to have a high copper surface area to achieve higher conversions but other factors can influence the activity.

It was evident that the presence of Zr promoted an increase in the copper surface area; however, this rise was not proportional to the Zr content. For example, the content of Zr in the CZAZr sample was lower than in the CZZr sample, which had a lower CO conversion. This finding indicated that the Al also has an important influence on the catalytic properties. Conversely, when comparing the catalysts prepared by the same method with and without Zr (LS-80 and CZAZr), the Cu surface area increased from 9.5 to 12.9 $m^2\ g^{-1}$, while the CO conversion increased from 14.3% to 37.6%. This result suggested that other factors were involved in the catalytic activity.

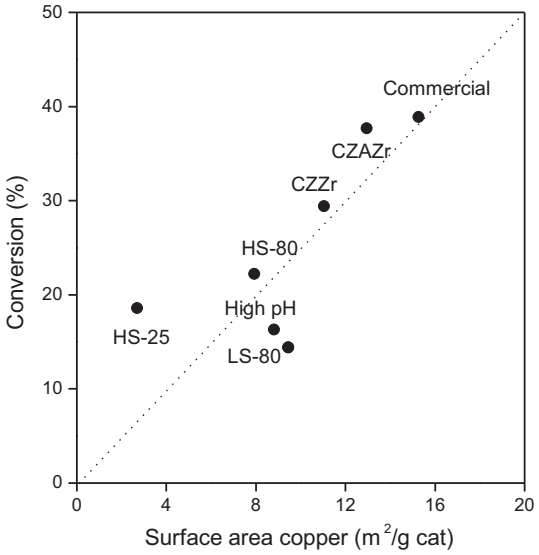

Fig. 7. Relation between metallic area vs. CO conversion.

The Zr promoter was not the only cause of the high conversion, as observed with the commercial sample. It was possible that a combination of properties was responsible for this activity. The high BET surface, small crystallite size and ease of reducibility were possible contributing factors. The amount of the hydroxycarbonated phase observed is tabulated in Table 2 (commercial sample). This was due to the memory effect of the hydrotalcite precursor, which resulted from the metal oxide phases being highly dispersed as a result of the high purity of this phase in this sample.

Fig. 8 shows the XRD patterns of the reduced samples. The complete reduction of CuO is illustrated by the metallic Cu peaks. The crystalline composition determined by the Rietveld method showed an absence of the CuO phase and the appearance of a ZrO_2 crystalline phase in the CZZr and CZAZr samples. Some differences were also observed in the intensity and broadness of the peak cor-

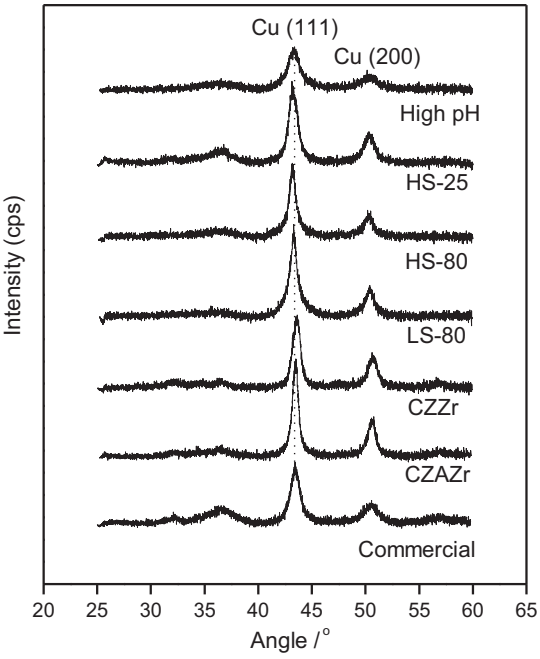

Fig. 8. XRD pattern of the reduced catalyst.

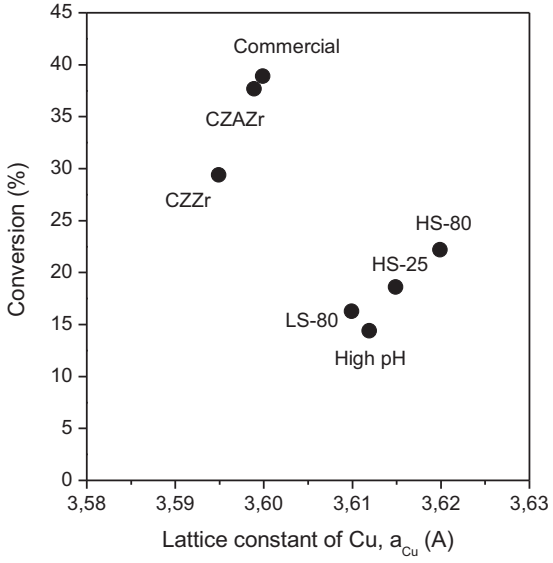

Fig. 9. Lattice constant *a* of Cu versus CO conversion.

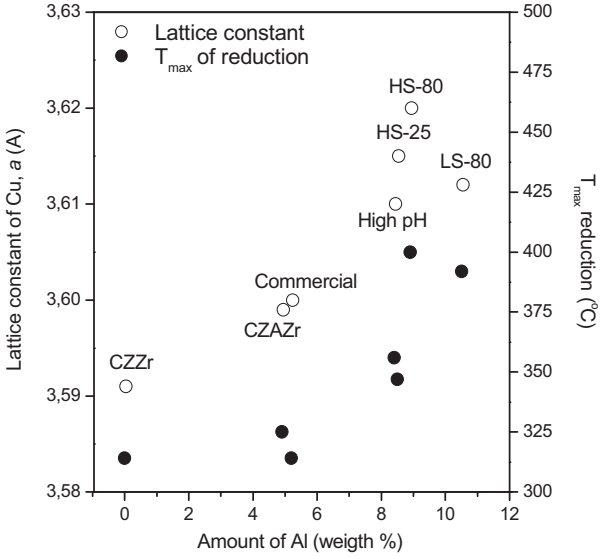

Fig. 10. Al content versus lattice constant of Cu and maximum temperature of reduction.

responding to the atomic plane of Cu (1 1 1), which was probably due to structural changes in the Cu matrix.

These structural changes were evident when the variation of the lattice constant *a* of Cu (1 1 1) was determined, as shown in Fig. 9. The results can be divided in two groups: the samples with Cu lattice constants above 3.610 Å and those with values below 3.60 Å. It can be concluded that the samples based on Cu–Zn–Al and prepared under different precipitation conditions presented an increase of the lattice constant under high supersaturation conditions. This increase was not enough to indicate the presence a Cu–Zn alloy because the lattice constant of pure Cu was 3.616 Å. It is important to mention that the values of the lattice constant obtained from XRD patterns of the reduced samples were not influenced by its *ex-situ* reduction.

A different interaction between Cu and ZrO_2 could be the cause of the structural changes observed in the samples based on Zr because it was not possible to have Zr in the Cu matrix, as it exhibits a very low solubility (Fig. 9). This view has been supported by Fisher and Bell [46] and other researchers [47–52]. The commercial sample did not contain Zr; however, it showed a higher conversion and high Cu surface area. Conversely, the linear dependence of the catalytic activity on the copper surface area was not general and was characteristic of a particular group of catalysts, some of which were obtained using similar preparation methods.

The Zr influenced the catalyst activity, but it was not solely responsible for the activity increase. The structural changes observed in Fig. 9 cannot be attributed to Zn in the Cu matrix because a lattice expansion was not observed, which is characteristic of Cu–Zn formation.

Some important promoter characteristics have been attributed to Zr by Sloczynskia and co-workers [36]; this included the addition of ZrO_2 to $Cu/ZnO/Al_2O_3$ and the complete replacement of Al_2O_3 by ZrO_2, which led to a distinct decrease of H_2O adsorption on these catalysts and an increase in the methanol yield. This effect had a positive influence on the hybrid catalyst performance because the presence of water on the surface of the catalyst inhibited the synthesis of methanol.

Based on the results observed in Fig. 9, it was possible to affirm that a relationship existed between activity and structure. However, it seemed that more than one factor influenced the structural changes observed in the catalysts. There was no evidence explaining why samples with low lattice constants of Cu presented higher conversions; however, it was not due to the formation of a Cu–Zn alloy.According to Velu and co-workers [53] as well as Breen and co-workers [44], the activity of a catalyst is directly related to the reducibility and the content of Al. The catalyst composition had an important influence on the physicochemical properties, such as copper reducibility, surface area and dispersion, which in turn influenced the catalyst performance. In this study, the catalytic activity improved with decreasing Al content. This theory made sense when the relationship between the Al content (weight %) and both lattice constant and maximum temperature of the reduction were considered (Fig. 10). It was possible to conclude from the results obtained that there was some degree of structural influence on the catalytic activity. Beyond the advantages known in the literature, Al could play a structural role that has not yet been observed.

5. Conclusions

It has been shown that metallic components influence the direct synthesis of DME from syngas. The role of this component was related directly to the CO conversion. The different precipitation conditions used to prepare the methanol synthesis catalyst influenced its textural and structural properties, but these changes did not influence the catalytic activity. Further, the Cu surface area found in the HS-25, HS-80, LS-80 and High pH catalysts had no direct correlation with the CO conversion. The smaller CO conversions were observed for these samples.

Catalysts based in Zr as the promoter also presented changes on the textural and structural properties and exhibited an increase in the metallic area and CO conversion; however, the increase on the activity was not proportional to the metallic sites and a synergetic effect due to structural changes seems to be responsible. The higher CO conversions were observed on catalysts based on Zr (CZZr and CZAZr). The CZAZr sample achieved a conversion as high as commercial sample but a higher selectivity toward DME. The higher CO conversions were observed on catalysts based on Zr. The CZAZr sample achieved a conversion comparable to the commercial sample but with a higher selectivity toward DME. An unexpected influence of the Al content on the structure of the methanol synthesis catalyst and the reducibility of CuO was observed and an important structural and catalytic role for Al should be considered.

Acknowledgment

We are grateful to PETROBRAS for financial support.

References

[1] D. Mao, J. Xia, Q. Chen, G. Lu, Catal. Commun. 10 (2009) 620.
[2] F. Dongmei, Z. Yizan, W. Dezheng, W. Jinfu, Chin. J. Catal. 30 (3) (2009) 223.
[3] A. Venugopal, J. Palgunadi, J.K. Deog, O.-S. Joo, C.-H. Shin, J. Mol. Catal. A: Chem. 302 (2009) 20.
[4] S.-H. Kang, J.W. Bae, K.W. Jun, H.S. Potdar, Catal. Commun. 9 (2008) 2035.
[5] J.-L. Li, X.-G. Zhang, T. Inui, Appl. Catal. A 147 (1996) 23.
[6] J.H. Kim, M. Park, O.S. Joo, K.D. Jung, Appl. Catal. A 264 (2004) 37.
[7] G.R. Moradi, S. Nosratu, F. Yaripor, Catal. Commun. 8 (2007) 598.
[8] A.T. Aguayo, J. Ereña, I. Sierra, M. Olazar, J. Bilbao, Catal. Today 106 (2005) 265.
[9] J. Ereña, R. Garoña, J. Arandes, A. Aguayo, J. Bilbao, Catal. Today 107–108 (2005) 467.
[10] T. Shishido, Y. Yamamoto, H. Morioka, K. Takehira, J. Mol. Catal. A: Chem. 268 (2007) 185.
[11] W.R.A.M. Robinson, J.C. Mol, Appl. Catal. 76 (1991) 117.
[12] Q. Ge, Y. Huang, F. Qiu, S. Li, Appl. Catal. A 167 (1998) 23.
[13] F.S. Ramos, A.M. Duarte de Farias, L.E.P. Borges, J.L. Monteiro, M.A. Fraga, E.F. Sousa-Aguiar, L.G. Appel, Catal. Today 101 (2005) 39.
[14] Q. Zhang, K. Asami, S. Asaoka, K. Fujimoto, Fuel Process. Technol. 85 (2004) 1139.
[15] J.H. Flores, M.I.P. da Silva, Colloids Surf. A (2008) 113.
[16] P. Prasad, J. Bae, S. Kang, Y. Lee, K. Jun, Fuel Process. Technol. 89 (2008) 1281.
[17] J.H. Flores, G. Solórzano, M.I.P. da Silva, Appl. Surf. Sci. 254 (2008) 6461.
[18] H.-B. Chen, D.-W. Liao, L.-J. Yu, Y.-J. Lin, J. Yi, H.-B. Zhang, K.-R. Tsai, Appl. Surf. Sci. 147 (1999) 85.
[19] T. Fujita, J. Nakamura, Catal. Lett. 56 (1998) 119.
[20] M. Günter, T. Ressler, B. Bems, C. Büscher, T. Genger, O. Hinrichsen, M. Muhler, R. Schlögl, Catal. Lett. 71 (2001) 37.
[21] J. Wagner, P. Hansen, A. Molenbroek, H. Topsøe, B. Clausen, S. Helveg, J. Phys. Chem. B 107 (2003) 7753.
[22] P. Hansen, J. Wagner, S. Helveg, J. Rostrup-Nielsen, B. Clausen, H. Topsøe, Science 295 (2002) 2053.
[23] L. Yong-Feng, D. Xin-Fa, L. Wei-Ming, Int. J. Hydrogen Energy 29 (2004) 1617.
[24] S. Velu, K. Suzuki, Top. Catal. 22 (2003) 235.
[25] J. Agrell, H. Birgersson, M. Boutonnet, I. Melián-Cabrera, R. Navarro, J. Fierro, J. Catal. 219 (2003) 389.
[26] H. Oguchi, H. Kanai, K. Utani, Y. Matsumura, S. Imamura, Appl. Catal. A 293 (2005) 64.
[27] A. Szizybalski, F. Girgsdies, A. Rabis, Y. Wang, M. Niederberger, T. Ressler, J. Catal. 233 (2005) 297.
[28] D.P.B. Peixoto, S.M. Cabral de Menezes, M.I. Pais da Silva, Mater. Lett. 57 (2003) 3933.
[29] C. Baltes, S. Vukojevic, F. Schuth, J. Catal. 258 (2008) 334.
[30] M. Mühler, L. Nielsen, E. Törnoqvist, B. Clausen, H. Topsoe, Catal. Lett. 14 (1992) 241.
[31] M. Turco, G. Bagnasco, U. Costantino, F. Marmottini, T. Montanari, G. Ramis, G. Busca, J. Catal. 228 (2004) 43.
[32] P. Guo, L. Chen, Q. Yang, M. Qiao, H. Li, H. Li, H. Xu, K. Fan, Int. J. Hydrogen Energy 34 (2009) 2361.
[33] P. Kurr, I. Kasatkin, F. Girgsdies, A. Trunchke, R. Schlögl, T. Ressler, Appl. Catal. A 348 (2008) 153.
[34] Y. Zhao, J. Chen, J. Zhang, J. Nat. Gas Chem. 16 (2007) 389.
[35] Y. Matsumura, H. Ishibe, Appl. Catal. B 91 (2009) 524.
[36] J. Słoczynskia, R. Grabowski, P. Olszewski, A. Kozłowska, J. Stoch, M. Lachowska, J. Skrzypek, Appl. Catal. A 310 (2006) 127.
[37] S. Velu, K. Suzuki, M. Okazaki, M. Kapoor, T. Osaki, F. Ohashi, J. Catal. 194 (2000) 373.
[38] M. Turco, G. Bagnasco, C. Cammarano, P. Senese, U. Costantino, M. Sisani, Appl. Catal. B 77 (2007) 46.
[39] S. Murcia-Mascarós, R.M. Navarro, L. Gómez-Sainero, U. Costantino, M. Nocchetti, J.L.G. Fierro, J. Catal. 198 (2001) 338.
[40] B. Lindström, L.J. Pettersson, P.G. Menon, Appl. Catal. A 234 (2002) 111.
[41] M. Liang, W. Kang, K. Xie, J. Nat. Gas Chem. 18 (2009) 110.
[42] M. Spencer, Surf. Sci. 192 (1987), 323, 329, 336.
[43] X.-M. Liu, G.Q. Lu, Z.-F. Yan, Appl. Catal. A 279 (2005) 241.
[44] J.P. Breen, J.R.H. Ross, Catal. Today 51 (1999) 521.
[45] W. Dow, W.Y. Wang, T. Huang, J. Catal. 160 (1996) 155.
[46] I.A. Fisher, A.T. Bell, J. Catal. 172 (1997) 222.
[47] T. Fujitani, J. Nakamura, Appl. Catal. A 191 (2000) 111.
[48] T. Fujitani, I. Nakamura, T. Uchijima, J. Nakamura, Surf. Sci. 383 (1997) 285.
[49] I. Nakamura, T. Fujitani, T. Uchijima, J. Nakamura, Surf. Sci. 400 (1998) 387.
[50] S.-I. Fujita, M. Usui, N. Takezawa, J. Catal. 134 (1992) 220.
[51] S.-I. Fujita, M. Usui, H. Ito, N. Takezawa, J. Catal. 157 (1995) 403.
[52] S.-I. Fujita, S. Moribe, Y. Kanamori, M. Kakudake, N. Takezawa, Appl. Catal. A 207 (2001) 121.
[53] S. Velu, K. Suzuki, M.P. Kapoor, F. Ohashi, T. Osaki, Appl. Catal. A 213 (2001) 47.